Journal Pre-proofs

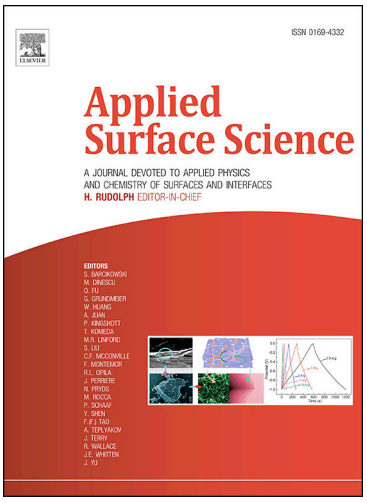

Full Length Article

Room temperature oxygen exchange and diffusion in nanometer-thick ZrO_2 and MoO_3 films

C.R. Stilhano Vilas Boas, J.M. Sturm, I. Milov, P. Phadke, F. Bijkerk

PII: S0169-4332(21)00460-8
DOI: https://doi.org/10.1016/j.apsusc.2021.149384
Reference: APSUSC 149384

To appear in: *Applied Surface Science*

Received Date: 9 November 2020
Revised Date: 4 February 2021
Accepted Date: 21 February 2021

Please cite this article as: C.R. Stilhano Vilas Boas, J.M. Sturm, I. Milov, P. Phadke, F. Bijkerk, Room temperature oxygen exchange and diffusion in nanometer-thick ZrO_2 and MoO_3 films, *Applied Surface Science* (2021), doi: https://doi.org/10.1016/j.apsusc.2021.149384

Room temperature oxygen exchange and diffusion in nanometer-thick ZrO_2 and MoO_3 films

C.R. Stilhano Vilas Boas Investigation Methodology Conceptualization Writing - Original Draft, J.M. Sturm Methodology Conceptualization Writing - Review & Editing Supervision Funding acquisition*,j.m.sturm@utwente.nl, I. Milov Formal analysis Writing - Review & Editing, P. Phadke Formal analysis Writing - Review & Editing, F. Bijkerk Writing - Review & Editing Supervision Funding acquisition

Industrial Focus Group XUV Optics, MESA+ Institute for Nanotechnology, University of Twente, Enschede, The Netherlands

Graphical abstract

Highlights

Isotope exchange observed in topmost few nm of oxide films exposed to O radicals.

Diffusion saturates in < 10 min, showing no influence of crystalline structure.

In depth saturation attributed to field-assisted diffusion in space charge layer.

Diffusion model calculates diffusion and surface exchange coefficients.

Adsorbed O species enhance diffusion by ~ 8 orders of magnitude compared to bulk.

Abstract

The diffusion of oxygen in thin films of ZrO_2 and MoO_3 was investigated with atomic ^{18}O as a tracer using low energy ion scattering sputter depth profiling. 3 nm amorphous and 20 nm polycrystalline films were prepared by reactive magnetron sputtering and exposed to atomic oxygen species at room temperature. Exposure results in a fast diffusion of oxygen to a limited depth of ~1 nm and ~2.5 nm for ZrO_2 and MoO_3, respectively, and surface exchange limited to a maximum of 65% to 75%. The influence of the crystalline structure of the films on exchange and diffusion was negligible. We propose that the transport of oxygen in oxides at room temperature is dominated by a field-induced drift, generated by the chemisorption of reactive oxygen species. The maximum penetration of oxygen is limited by the oxide space charge region, determined by the oxide electrical properties. We applied a drift-diffusion model to extract values of surface potential and kinetic parameters of oxygen exchange and diffusion. The developed experimental analysis and modelling suggest that the electric field and consequent distribution of charged species are the main factors governing exchange rates and species diffusion in an oxide thin film at room temperature.

Keywords: Isotope exchange, Thin films, Space charge layer, Transition metal oxides, Low temperature, Low energy ion scattering

1. Introduction

With the advance in nanometer-thick film synthesis, the application of transition metal oxides has exponentially grown. As thin films, they are employed in a wide range of functions, from electrodes in solid oxide fuel cells [1] and charge injection layers in organic electronics [2], to protective layers against corrosion and for increase of components lifetime [3]. In most of these applications, the interaction between the oxide surface and atmospheric species, such as oxygen, is present. The majority of studies in that context focused on molecular oxygen-oxide interaction at high temperatures (T > 300ºC), in which it is commonly accepted that the chemisorption and incorporation of oxygen into the oxide lattice results in change of oxide properties [4-8]. However, little is known on the effect of atomic oxygen species interacting with oxide surfaces at moderate temperatures, i.e. close to 25ºC (about room temperature) [9].

The aim of the present work is to understand the mechanisms governing the interaction of atomic oxygen with oxides at room temperature. The understanding of such interaction is critical considering applications where oxides are not directly exposed to high temperatures, but processes such as exposure to ultraviolet light [10,11] or electron beam [12,13] might induce the formation of atomic oxygen species at oxide surfaces. Transport of oxygen in an oxide lattice is initiated by oxygen exchange at the surface, followed by diffusion to sub-surface regions. The diffusion can be along grain boundaries (commonly assumed to be a faster diffusion pathway [14]) or bulk [15]. For molecular species in contact with binary oxides at room temperature, it is reported that the surface oxygen exchange is quenched, as the low temperature and the lack of high defect or dopant concentration prevents the reaching of the energy required to surpass the activation barrier of molecular dissociation [16,17]. However, in case of exposure to atomic or radical species, the absence of the molecular dissociation step might enable the interaction to proceed to the lattice transport phase. This transport might affect the system in which an oxide is employed, for example by inducing changes in the oxide properties or by affecting layers that are supposed to be protected by the oxide (especially relevant when oxides are employed as diffusion barrier materials). Therefore, a better understanding of the nature of the interaction between atomic oxygen and oxide at low temperatures is of immediate importance for relevant technological applications of oxides.

One of the most powerful methods for studying oxygen transport processes is the so-called Isotope Exchange Depth Profile (IEDP). This technique consists of the combination of exposure of an oxide to the isotope ^{18}O, followed by in-depth analysis of the isotope profile by sputter depth profiling with an ion beam technique. Typically, secondary ion mass spectrometry (SIMS) is applied in IEDP analysis, as it provides a direct measure of oxygen transport kinetic parameters [18]. However, SIMS profiles lack precise information about the surface chemistry and oxygen exchange in thin films in the nanometer range, due to its large information depth (between 4 and 7 monolayers depth) [18]. In this context, the low-energy ion scattering (LEIS) technique provides the opportunity of correlating exchange kinetics with chemical processes at the topmost atomic layers of materials, giving an unprecedented level of information on surface

exchange and diffusion in oxides with isotopic discrimination [18,19]. Therefore, the detailed analysis with LEIS-IEDP allows one to unambiguously discern between the mechanisms involved in lattice diffusion and surface exchange processes, together with determining the respective transport parameter characteristics of each mechanism [15,18].

In the present study, we apply LEIS-IEDP to verify the interaction between atomic oxygen and thin film oxides of zirconium (ZrO_2) and molybdenum (MoO_3), with different thicknesses and crystalline structures. These materials were chosen to allow a comparison between a metal that only forms a single stable stoichiometric oxide (Zr) and a prototypical metal that can form various stable bulk oxidation states (Mo). Deposition by reactive magnetron sputtering, atomic O exposure and LEIS analysis were carried out *in-vacuo*, which enables to extract the precise time evolution of isotope surface exchange and in-depth diffusion without the interference of surface contaminants. Our analysis suggests that the formed isotope profiles are a consequence of the field formed upon chemisorption of reactive oxygen species at the oxide surface and associated accumulation of charged species near the surface (upward band bending). This process induces exchange and increases diffusivity of oxygen in the space charge region of the oxide. By applying a drift-diffusion model, we extract relevant kinetic parameters and suggest main factors that may influence oxygen diffusion.

2. Experimental

The experiments were performed in a home-designed ultrahigh vacuum system at a base pressure of $\leq 1 \times 10^{-9}$ mbar, which allows in-vacuum transfers between deposition (magnetron sputtering), characterization (LEIS and X-ray photoelectron spectroscopy (XPS)) and oxygen exposure chambers with negligible surface contamination. Films of 20 nm and 3 nm of ZrO_2 and MoO_3 were obtained by reactive direct current (DC) magnetron sputtering of the respective metallic target with a mixture of oxygen and argon. The samples were deposited on a 25 x 25 mm^2 Si(100) substrate with a native oxide layer. The average deposition pressure was 5×10^{-4} mbar and the growth rate was typically 0.05 nm/s. The stoichiometry of deposited films was verified by XPS experiments with a Thermo Theta Probe spectrometer, using Al-Kα radiation.

For a complete analysis of oxygen-oxide interaction, we performed three types of oxygen exposure: (i) exposure to molecular tracer oxygen ($^{18}O_2$) for testing of oxide surface stoichiometry; (ii) exposure to atomic ^{18}O (isotopic enrichment 98%) to perform isotope tracing analysis; (iii) exposure to atomic ^{16}O to check the reversibility of obtained isotopic profiles. All exposures were performed at room temperature with background O_2 partial pressure of 1×10^{-4} mbar. The atomic species were generated by a Specs MPS-ECR mini plasma source, with atomic oxygen flux in the order of 10^{15} atoms/cm^2/s. The exposure time ranged between 10 s and 2400 s, and an IEDP analysis was performed after each exposure period. Isotope exchange depth profiles were obtained by performing LEIS sputter depth profiling on the exposed samples. In this analysis mode, each sputter step is followed by a LEIS analysis according to the acquisition

parameters described below.

LEIS measurements were performed in an ION-TOF GmbH Qtac^{100} high sensitivity LEIS spectrometer, described in detail elsewhere [20]. A He^+ ion beam at 3 keV energy and 2.5-3.5 nA current, measured before each spectrum acquisition in a Faraday cup, was chosen for characterization. The typical ion fluence directed at the sample was 2×10^{14} He^+ ions/cm^2, with a total acquisition time of 3 minutes. Using these analysis parameters, artifacts such as ion-induced sputtering and intermixing are negligible. Sputter depth profiling was done with a sputter gun attached to the LEIS chamber, positioned at 59^o with respect to the sample surface normal, applying a 0.5 keV Ar^+ beam at 100 nA average current. The sputtered area was fixed at 2×2 mm^2. The sputtered depth was calculated by verifying the necessary ion dose (at the specified energy) to sputter through a reference oxide sample with known thickness (determined by X-ray reflectometry).

The X-ray reflectometry measurements were performed using a PANalytical Empyrean X-ray diffractometer (Cu-Kα radiation, 0.154 nm). The same equipment was applied in X-ray diffraction (XRD) mode, using in-plane grazing incidence XRD (GIXRD) geometry at a fixed incident angle (higher than the critical angle) to determine the structures of deposited films.

3. Results

To verify a possible influence of atomic arrangement on the process of oxygen-oxide interaction, the crystalline structure of the deposited films was characterized by X-ray diffraction. Figure 1 shows XRD measurements of reactively deposited thick and thin oxides. The main peak of 20 nm ZrO_2 is related to the monoclinic phase [21], and the three peaks of 20 nm MoO_3 correspond to the orthorhombic (α-MoO_3) phase [22]. Thin oxides with a thickness of 3 nm do not show any characteristic oxide peaks, being therefore amorphous. Since the detection of crystallinity in few nm thick films by XRD may be difficult due to the small volume of material, the 3 nm ZrO_2 film was also investigated by transmission electron microscopy, which confirmed the amorphous nature of this oxide film. The broad features around a 2θ value of 50° are related to the Si(100) substrate and typically appear for thin oxide films.

It is known from literature that at room temperature the stoichiometric surfaces of ZrO_2 and MoO_3 are chemically inert to O_2 interactions [17,23]. In order to verify the reactivity of the deposited oxide layers towards molecular oxygen, we exposed the films of 3 and 20 nm of ZrO_2 and MoO_3 to molecular isotopic oxygen ($^{18}O_2$) for 25 min. Figure 2 shows as an example the obtained LEIS signals for the as deposited and $^{18}O_2$ exposed 3 nm films. Both spectra show characteristic surface peaks of ^{16}O (indicated by the dashed line) and metal atoms (around 2500 eV) at the surface. The broad tail feature at the low energy side of the metal surface peak is related to scattering on sub-surface metal atoms [19]. The oxide films exposed to molecular isotopic oxygen exhibit no characteristic ^{18}O peak (see dashed line labeled with ^{18}O for the

expected position from reference measurements). The LEIS signals from thick 20 nm films (not shown) exhibit similar behaviour. This analysis demonstrates that the as deposited surfaces can be considered as stoichiometric with a low defect concentration.

On the contrary, exposure to atomic ^{18}O radical species leads to exchange of isotopic oxygen in metal oxide films. Figure 3 compares the LEIS signal from 20 nm MoO_3 before and after the exposure to isotopic atomic oxygen species. It is worth noting that the exposure does not significantly change the intensity of the metal peak, which is observed for all analyzed materials. With this, we can conclude that the observed ^{18}O peak corresponds to atoms that replaced ^{16}O in the topmost atomic layer, and not to additional oxygen species adsorbed on top of the surface metal atoms. This fact is in agreement with previous studies that revealed lattice exchange as the dominating diffusion mechanism in binary oxides [24].

Following this initial analysis, IEDP was performed for all samples. Figure 4 shows the obtained profiles of ^{18}O relative concentration for the different samples and exposure times as a function of sputtered depth, and Figure 5 shows the surface concentration evolution with exposure time. Here we represent the ^{18}O concentration by the ratio of the atomic fraction of this oxygen isotope to total oxygen (i.e., $^{18}O/(^{18}O + ^{16}O)$). The atomic fractions were determined by using a pure metal oxide as reference in order to avoid the influence of matrix effects [25] and with appropriate corrections of the ^{18}O signal for differences in sensitivity factor compared to ^{16}O [26]. No significant difference in the obtained profiles is observed between thin amorphous and thick polycrystalline samples. A slight difference in final oxygen diffusion depth (~ 1 monolayer depth, or < 0.5 nm) observed between amorphous and polycrystalline films is within systematic uncertainty (estimated as 0.3 nm for ZrO_2 and 0.4 nm for MoO_3). Likewise, a slight change on decay behavior of isotopic concentration can be perceived between the topmost and deeper layers of the oxides (at ~0.25 nm depth for ZrO_2 and ~0.4 nm depth for MoO_3), which may point at different diffusion behavior in the topmost layer, as reported before for higher temperature diffusion experiments [27]. However, considering the uncertainty of both depth and isotopic concentration and the very small depth range (in the range of single atomic layers) for which changes in diffusion constant might occur, the profiles are assumed to correspond to single diffusion regimes for all cases.

One can see that in all cases the outermost surface and in-depth concentration of ^{18}O gradually increases with exposure time, until saturation is reached. After that, further exposure does not lead to considerable increase in isotope concentration. The saturation of surface exchange occurs at about 65% to 75% for all samples, while the maximum diffusion depth of isotopes is ~ 1 nm for ZrO_2 and ~ 2.5 nm for MoO_3. The saturation time is equal to ~100 s for ZrO_2 and 450 s for MoO_3. No difference in preferential sputtering due to incorporation of ^{18}O was observed [28], as verified by comparing the evolution of total oxygen concentration between exposed and as deposited samples.

The reversibility of the transport profiles was checked by consecutive exposures to ^{16}O and ^{18}O. Initially, the as-deposited oxide films were exposed to ^{16}O atoms (for 2400 s). The film was subsequently exposed to ^{18}O atoms and analyzed by LEIS-IEDP. These samples presented the same isotopic evolution as presented in Figures 4a-d. After this, the same samples were again exposed to ^{16}O. The profiles were shown to be reversible (i.e. ^{18}O was replaced by ^{16}O) and not affected by the consecutive exposures. The performed experiments indicate that it is unlikely that the saturation and evolution of the surface exchange and in-depth concentration profiles are governed by a possible substoichiometry of the (surface layer) of the as-deposited films.

4. Discussion

Previous investigations of thin metal films exposure to atomic oxygen at room temperature showed that Mo and Zr form oxide films with a limited thickness of about 4 and 5.5 nm, respectively, after which further growth of oxide ceases [29]. As first explained by Cabrera and Mott [30], oxygen and/or metal transport across thin oxide films at low temperature is assisted by an electric field generated between adsorbed (electronegative) O species at the surface and the metal underneath. As the oxide film thickness grows, the electric field across the oxide decreases, until it becomes too low to induce diffusion. Since thermal diffusion is negligibly small at this temperature, the growth processes ceases. Therefore, at first glance it may seem surprising that oxygen diffusion at room temperature occurs in fully oxidized metal oxide films. However, for metal oxides, it is reported in literature that surface phenomena such as adsorption, can also lead to a generation of an electric field at the oxide surface [12,31]. For n-type oxides, such as MoO_3 and ZrO_2 [32,33], when an acceptor specie approaches the surface, the unfilled orbital of the specie extracts electrons from the oxide. The accumulation of negatively charged species at the oxide surface induces the formation of an electric field near the surface. The low free carrier density and poor screening length in the oxide impede the screening of the formed electric field, which leads to charge redistribution and creates a space charge region (SCR) near the oxide surface [12]. Upon the adsorption of acceptor species, electrons are depleted from the surface (accumulation of positive charges), which leads to an upward shift of the energy band edges at the oxide surface. For a donor specie, the opposite effect occurs and a downward band bending is observed. This phenomenon is analogous to the process described by Schottky and Mott on metal/semiconductor interfaces [12,34].

We propose that the adsorption of atomic oxygen induces the formation of an electric field and, consequently, the formation of an SCR at the near-surface region of both oxides studied. Since atomic oxygen is an acceptor specie, a negative field is generated (upward band bending). This field assists the diffusion of mobile oxygen, metal and/or vacancy species within the SCR, thereby explaining significant oxygen diffusion in the topmost few nanometer of the film. It was previously reported in literature [16,35] that the interaction between molecular oxygen (at relatively high pressures) and ozone with n-type oxides at room temperature leads to an upward band bending. In the work by Nowotny [16], it is argued that oxygen rapidly chemisorbs to the surface, forming singly ionized molecular and atomic species, which slowly diffuse into the oxide. Lampimäki et al. [35] demonstrated with high-pressure XPS analysis that titanium and iron oxides when exposed to ozone generate an SCR - and a resulting electric field - of only few nanometer thickness. However, the process of isotope exchange was not explored in these studies. For our analysis, we take into consideration these previous studies and assume the experimentally observed isotopic diffusion depth to be related to the electric field within the oxide SCR. With that, we applied a drift-diffusion model to obtain values of band bending, charge defect density and kinetic parameters of diffusion for all analyzed cases.

4.1. Drift-diffusion model for RT isotopic exchange

Using a description analogous to the one applied by De Souza [36], one possible pathway for the forward exchange reaction between oxide and atomic oxygen can be given as:

$$O \xrightarrow{+e^-} O^-_{chem} \xrightarrow{+e^- + V_{\ddot{O}}} O^{2-}_{x=0} \xrightarrow{T+E} O^{2-}_{\lambda} \xrightarrow{T} O^{2-}_{bulk}. \qquad (1)$$

The atomic specie chemisorbs (subscript chem) to the oxide surface and reacts with an oxygen vacancy placed on the outermost layer of the oxide (x = 0), penetrating the film. The charged ion is then transferred through the space charge region ($0 < x < \lambda$), with thermal (T) and field-induced (E) mechanisms influencing the atomic motion. Finally, the oxygen will diffuse in the bulk of the oxide (considered here as the region beyond the space charge layer, x = bulk), where charge distribution is assumed to be neutral and only thermal processes are considered [37].

The transport equation that describes the entirety of the diffusion process is obtained by implementing a field-driven (drift) term to the Fickian-type diffusion equation, as described in (2):

$$\frac{\partial C^*(x,t)}{\partial t} = D_e^* \nabla^2 C^*(x,t) - \mu \vec{E} \nabla C^*(x,t) \quad ()$$

where C^* is the atomic fraction of tracer ^{18}O [38], referred in the text as "isotopic concentration" for simplicity, q is the charge on the diffusing ion (*-2e* for oxygen, with e being the electronic charge), μ is the ionic mobility, t is the exposure time and x is the depth. The mobility μ can be approximated by the Nernst-Einstein's relation $\mu = (qD_i^*)/k_bT$, where k_b is the Boltzmann constant and T is the absolute temperature [39]. D_i^* represents the intrinsic diffusion coefficient of oxygen species in the oxide, i.e. without influence of charge effects. Therefore, D_i^* can be approximated to the thermal self-diffusion coefficient of oxygen in the oxide lattice at room temperature [40,41]. The theoretical analysis developed by Yang et al. [42] suggests that, at low O_2 pressures, the oxygen self-diffusion coefficient at room temperature for single-crystal monoclinic ZrO_2 should be in the order of 10^{-30} m^2 s^{-1}. A similar study was not found for MoO_3. However, with similar values for defect formation and oxygen binding energies for ZrO_2 and MoO_3 presented in literature [43,44], we assumed D_i^* of both oxides to be in the same order of magnitude. The coefficient D_e^* designates the field-enhanced diffusivity at the space charge region. This concept was initially pointed-out in our previous study on the diffusion of energetic oxygen ions in transition metals [40]. In the present case, we extend the previous analysis and determine values for D_e^* based on formalism demonstrated by Meyer et al. [45] and further developed by De Souza et al. [46], correlating the field-enhanced diffusivity to the expected surface potential generated by the oxygen-oxide interaction:

$$D_e^* \approx D_i^* e^{\frac{q\{\Phi_0 - \Phi_b\}}{k_b T}} \quad (),$$

where Φ_0 and Φ_b respectively represent the electrostatic potential at the surface and in the bulk.

The electric field distribution $\vec{E}$ was obtained by solving Poisson's equation. Considering that the charge density in the space charge layer is not influenced by the ion exchange (the charge density only refers to stoichiometry defects, and it is assumed that the exposure to atomic oxygen does not change the oxide stoichiometry, as also validated by our experiments), the time-independent form of Poisson's equation can be used:

$$\nabla\vec{E} = \nabla^2\Phi = -\frac{\rho(x)}{\varepsilon \cdot \varepsilon_0} \quad (2),$$

where $\rho(x)$ is the space charge density, ε_0 is the vacuum permittivity and ε is the relative permittivity of the oxide. In this study, we apply Schottky's approximation to solve Poisson's equation [12,46,47]. In this approximation, the charges are assumed to be homogeneously distributed in the SCR with a density of N_d, while the potential is set to a fixed value at the surface (Φ_0) and zero in the bulk (Φ_b). As previously mentioned, in our analysis we assume the experimentally observed maximum diffusion depth of isotopes to be equivalent to the thickness of the SCR.

Finally, the solution of Equation (2) requires an initial condition and two boundary conditions to be determined. The right boundary is set as $\nabla C^*|_{x\to\infty} = 0$, and for the left boundary we assume that the net injected flux of tracer species (j_{18}^{in}) obeys Fick's first law:

$$j_{18}^{in} = k_e^* \left(C_g^* - C^*(x=0,t)\right) \quad (3),$$

where k_e^* is the effective surface exchange coefficient [46,48,49], $C^*(s,t)$ is the surface tracer concentration at time t, and C_g^* is the isotope fraction in the gas. Values of ε were based on literature [50], while N_d and the surface potential Φ_0 were obtained from the best fit of the system of Equations 2 to 5 to experimental results [31,50-53].

4.2. Model implementation and analysis of parameters

Based on the described model and mentioned assumptions, we applied a numerical finite difference method to solve the system of differential equations and obtain the values for N_d, Φ_0 and k_e^* with best fit to the observed diffusion profiles. Table 1 shows the best fit values of N_d, Φ_0 and k_e^*, and the corresponding values of SCR and D_e^* for all cases. Figure 4 and Figure 5 compare the experimental and calculated values

for in-depth saturation profile and surface concentration evolution, respectively. It is seen in Figure 4 that the profiles calculated for 100 s exposure of ZrO_2 and 450 s exposure of MoO_3 are in agreement with the obtained experimental data. However, the model does not justify the experimentally observed saturation of the diffusion profiles (i.e. variation of oxygen concentration in depth). That is, for longer periods of exposure, the model predicts an increase of isotopic concentration within the SCR. Similarly, in Figure 5, the theoretical model also predicts a continued increase of oxygen exchange (close to unity) with exposure time, which is not confirmed experimentally.

The calculated results are sensitive to the set of parameters used. Therefore, we continue the discussion by exploring the validity of the assumptions taken for solving the system of equations, and the consequent parameters obtained by the fitting. For that, we compare the obtained results with data previously reported in literature. We also look into the possible reasons for the experimentally observed saturation of oxygen exchange and diffusion.

We begin with addressing the saturated maximum diffusion depth of isotopes and the obtained values of charged carrier concentration. One key point of our analysis lies in the assumption that the maximum diffusion depth of isotopes is directly linked to the thickness of the SCR. From this assumption, we obtain values of N_d higher than typically reported values of bulk charge carrier concentration of undoped oxides [12]. An important observation, however, is that according to the generalized treatment of space charges at interfaces in crystalline solids, the concentration of charged species in the SCR might differ considerably from the bulk, especially when the surface is exposed to strongly oxidizing conditions or in the presence of surface potentials [46,54,55]. This initial assumption for maximum diffusion depth also influences the obtained values of Φ_0 and, consequently, D_e^*. However, the values of Φ_0 shown in **Error! Reference source not found.** are in agreement with measurements of the shift in electronic states for different n-type oxides exposed to molecular oxygen and ozone at room temperature, reported ranging from 0.2 eV to 0.9 eV [16,35]. Additionally, the comparison between the diffusion of oxygen observed in this study and previous analysis in literature [23,56–58] provides a strong indication that the in-depth diffusion kinetics is mainly determined by the surface potential generated from the oxygen adsorption. If only thermal processes and concentration gradients would act as driving force for diffusion, we imagine that one of the two following scenarios would be detected: i) the oxygen diffusion would not surpass the outermost oxide layer in the analyzed timeframe (since the reported bulk diffusion constants of oxygen in the studied oxides are in the order of 10^{-30} m^2 s^{-1} at room temperature [42]); or ii) in case our deposited films had a much higher thermal/bulk diffusion constant than reported reference values, the profile would not saturate within a limited diffusion depth. Finally, it is interesting to note that the obtained values of D_e^* are similar to the estimated field-induced diffusion term described in our previous oxygen ion diffusion study [40]. This might be an indication that the space charge layer formation and field build-up on oxides is present whenever atomic species are in contact with the oxide surface, independent of the initial state of the oxygen specie to

which the sample is exposed to. We would like to point out, however, that the assumed bulk-diffusivity directly influences the derived values of surface potential and diffusion constants. So the obtained values should be considered as realistic estimates. Furthermore, the comparable oxygen diffusion in both amorphous and crystalline oxides indicates a negligible influence of structure on the exchange and diffusion of oxygen at room temperature. This negligible structure dependence can be most likely explained since the diffusion at room temperature is almost completely field induced. Changes in (crystalline) structure of the material will influence thermal diffusion, but have no or limited effect on electrical properties of the oxide and the field induced in the space charge layer. Similarly, no effect of crystalline structure of thin metal films on room temperature oxidation by atomic oxygen was observed in a previous study [29]. With similar values of surface potential obtained for MoO_3 and ZrO_2, the lower permittivity of ZrO_2 results in the formation of a thinner SCR. Such an effect was also observed in the comparison between SCR depths of Fe_2O_3 and TiO_2 [35]. This fact supports the hypothesis of the oxygen exchange and diffusion processes to be mainly dominated by the material electronic properties.

The limited surface exchange and diffusion profile observed in practice can be related to several causes. It is reported in literature [35] that space charge effects might also lead to a limited surface coverage of the adsorbed oxygen species, influencing the concentration of isotopic species available for exchange. Other sources for the limited saturation may be a limited isotopic purity (e.g. caused by exchange reactions between ^{18}O atoms with ^{16}O atoms on oxide materials in the plasma source) and the presence of oxygen atoms on the surface that do not participate in exchange reactions. Unfortunately, there is no possibility to probe experimentally the isotopic purity of our atomic oxygen source. However, a restriction of the maximum surface isotope concentration to 80% in the calculation (grey dotted curves in Figure 5) for both oxides leads to a better agreement of surface exchange values between model and experimental data for higher exposure times. Nevertheless, this assumption is not enough to exactly reproduce the experimentally observed saturation of the exchange and diffusion profiles. This indicates a higher complexity of the dynamics of surface exchange and diffusion processes, for instance due to deviations of the diffusion behavior in the topmost atomic layers, as discussed before, which are not covered by the adopted model.

In view of the above discussion, we propose the oxygen-oxide interaction at room temperature to proceed as schematized in Figure 6: the atomic oxygen specie (^{18}O in the present case), when in contact with the oxide, becomes negatively charged and induces the formation of a depletion layer at the oxide surface and consequently a negative field (pointing in the direction from the substrate towards the surface). This field promotes both inward diffusion of negatively charged oxygen and upward redistribution of positively charged species near the surface. Meanwhile, surface reactions between adsorbed oxygen (^{18}O)

and oxygen on the surface (^{16}O) may occur, e.g. through exchange of O on coordinately unsaturated sites with O on regular lattice sites, or by reactions of O radicals with surface O atoms, resulting in O_2 desorption, thereby generating vacancy sites that promote O adsorption and, consequently, isotopic exchange. Therefore, the formed SCR represents a highly reactive region where isotope exchange is observed. In the context of room temperature exposure of oxides to atomic oxygen, the exchange and diffusion are dominated by the field-induced drift, and contrary to oxides exposed to molecular oxygen [16], the incorporation is fast, as the limiting step of molecular dissociation is not present. The depth and dynamics of exchange will be mainly dependent on the electric properties of the oxide, with negligible influence of crystalline structure. This would justify the reversible near-surface behavior for both thin and thick ZrO_2 and MoO_3. Comparatively, in our previous study on the oxidation of thin metal films by atomic oxygen at room temperature (where non-oxidized metal was present below the formed oxide film) [29], we have identified the depth of the isotope diffusion to be greater than observed in the present analysis. This increased isotope diffusion might be attributed to the influence of the Cabrera-Mott field that drives oxide growth. Typical Cabrera-Mott fields are in the order of 10^9 V/m [59], which is at least an order of magnitude larger than the fields expected in the space charge region of oxide films characterized in the present work. This phenomenon appears as an interesting fact to be further investigated regarding the role of the space charge in the kinetics of metal oxidation and oxygen transport in thin films.

5. Conclusion

Our study demonstrates the room temperature oxygen exchange and diffusion in amorphous and polycrystalline films of zirconium (ZrO_2) and molybdenum (MoO_3). The results show that, for all analyzed oxide films, oxygen exchange and diffusion reach saturation in a few minutes (< 10 min). The isotopes were found at maximum depth of approximately 2.5 nm for MoO_3 and 1 nm for ZrO_2. The surface exchange reached a maximum of 65% to 75% for all the analyzed samples. Our analysis suggests that, due to its acceptor nature, atomic oxygen becomes negatively charged when in contact with the oxide surface. The accumulation of negatively charged species at the oxide surface induces the formation of an electric field, and as a result a space charge region is formed. We found that these processes are determining factors for the diffusion of oxygen at low temperatures. The generated field is responsible for the increase in diffusion coefficient, whereas the saturation of exchange and diffusion are most likely related to the space-charge layer thickness and distribution of charged species in the analyzed thin films. The oxide structure, however, does not play a role in oxygen diffusion at the experimental conditions considered. By applying a drift-diffusion model, we obtained values of surface potential, and exchange and diffusion coefficients for the films analyzed. All oxides presented similar values of surface potential (~0.28 V), with effective diffusion and exchange coefficients varying from 5.5×10^{-22} to 9.1×10^{-21} m^2/s and from 2.3×10^{-12} to 4.5×10^{-12} m/s respectively. We discussed the implications of charge dynamics to the applied diffusion model, revealing that the existing models might be insufficient to completely describe the complex dynamics of oxygen

transport in oxides at low temperatures.

This study indicates that the presence of molecular dissociation processes (such as exposure to ultraviolet light or electron beam), or application of an external electric field might lead to higher exchange rates and species diffusion in an oxide thin film. Furthermore, we demonstrate LEIS-IEDP as a robust method for determining surface exchange and diffusion under exposure conditions where interaction results in fast near-surface processes.

Declaration of competing interests

The authors declare that they have no known competing financial interests or personal relationships that could have appeared to influence the work reported in this paper.

Acknowledgements

This work is part of HTSM project 13913, funded by NWO Applied and Engineering Sciences with co-funding by Carl Zeiss SMT. The authors also acknowledge the Industrial Focus Group XUV Optics at the MESA+ Institute at the University of Twente, as well as the Province of Overijssel.

References

[1] R.M. Ormerod, Solid oxide fuel cells, Chem. Soc. Rev. 32 (2003) 17–28. https://doi.org/10.1039/b105764m.

[2] J. Fahlteich, M. Fahland, W. Schönberger, N. Schiller, Permeation barrier properties of thin oxide films on flexible polymer substrates, Thin Solid Films. 517 (2009) 3075–3080. https://doi.org/10.1016/j.tsf.2008.11.089.

[3] Y. Sasaki, M. Kawamura, T. Kiba, Y. Abe, K.H. Kim, H. Murotani, Improved durability of Ag thin films under high humidity environment by deposition of surface Al nanolayer, Appl. Surf. Sci. 506 (2020) 144929. https://doi.org/10.1016/j.apsusc.2019.144929.

[4] U. Brossmann, G. Knöner, H.E. Schaefer, R. Würschum, Oxygen diffusion in nanocrystalline ZrO2, Rev. Adv. Mater. Sci. (2004). https://doi.org/10.1002/chin.200442249.

[5] H. Schmalzried, Diffusion in oxides, React. Solids. 5 (1988) 269–278. https://doi.org/10.1016/0168-7336(88)80026-3.

[6] G. Bakradze, L.P.H. Jeurgens, T. Acartürk, U. Starke, E.J. Mittemeijer, Atomic transport mechanisms in thin oxide films grown on zirconium by thermal oxidation, as-derived from 18O-tracer experiments, Acta Mater. 59 (2011) 7498–7507. https://doi.org/10.1016/j.actamat.2011.08.035.

[7] P. Kofstad, Nonstoichiometry, diffusion, and electrical conductivity in binary metal oxides., Wiley-Interscience, 1974. https://doi.org/10.1002/maco.19740251027.

[8] M.T. Greiner, L. Chai, M.G. Helander, W.M. Tang, Z.H. Lu, Transition metal oxide work functions: The influence of cation oxidation state and oxygen vacancies, Adv. Funct. Mater. 22 (2012) 4557–4568. https://doi.org/10.1002/adfm.201200615.

[9] K. Sasaki, J. Maier, Low-temperature defect chemistry of oxides. I. General aspects and numerical calculations, J. Appl. Phys. 86 (1999) 5422–5433. https://doi.org/10.1063/1.371541.

[10] R. Kevorkyants, M.N. Sboev, Y. V. Chizhov, Ab initio R1 mechanism of photostimulated oxygen isotope exchange reaction on a defect TiO2 surface: The case of terminal oxygen atom exchange, Appl. Surf. Sci. 403 (2017) 342–346. https://doi.org/10.1016/j.apsusc.2017.01.116.

[11] M. Tsuchiya, V. Shutthanandan, M.H. Engelhard, S. Ramanathan, Direct measurement of oxygen incorporation into thin film oxides at room temperature upon ultraviolet photon irradiation, Appl. Phys. Lett. 93 (2008) 163109. https://doi.org/10.1063/1.3058691.

[12] Z. Zhang, J.T. Yates, Band bending in semiconductors: Chemical and physical consequences at surfaces and interfaces, Chem. Rev. 112 (2012) 5520–5551. https://doi.org/10.1021/cr3000626.

[13] I. Popova, V. Zhukov, J.T. Yates, Electron-stimulated conversion of chemisorbed O to Al2O3on Al(111), Appl. Phys. Lett. 75 (1999) 3108–3110. https://doi.org/10.1063/1.125246.

[14] H. Schraknepper, R.A. De Souza, Competing descriptions of diffusion profiles with two features: Surface space-charge layer versus fast grain-boundary diffusion, J. Appl. Phys. 119 (2016). https://doi.org/10.1063/1.4941555.

[15] R.A. De Souza, R.J. Chater, Oxygen exchange and diffusion measurements: The importance of extracting the correct initial and boundary conditions, Solid State Ionics. 176 (2005) 1915–1920. https://doi.org/10.1016/j.ssi.2005.05.010.

[16] J. Nowotny, T. Bak, L.R. Sheppard, M.K. Nowotny, Reactivity of titanium dioxide with oxygen at room temperature and the related charge transfer, J. Am. Chem. Soc. 130 (2008) 9984–9993. https://doi.org/10.1021/ja7108695.

[17] V.E. Henrich, P.A. Cox, The surface science of metal oxides, Cambridge University Press, 1996.

[18] J.A. Kilner, S.J. Skinner, H.H. Brongersma, The isotope exchange depth profiling (IEDP) technique using SIMS and LEIS, J. Solid State Electrochem. 15 (2011) 861–876. https://doi.org/10.1007/s10008-010-1289-0.

[19] H.H. Brongersma, M. Draxler, M. de Ridder, P. Bauer, Surface composition analysis by low-energy ion scattering, Surf. Sci. Rep. 62 (2007) 63–109. https://doi.org/10.1016/j.surfrep.2006.12.002.

[20] A.A. Zameshin, A.E. Yakshin, J.M. Sturm, H.H. Brongerma, F. Bijkerk, Double matrix effect in Low Energy Ion Scattering from La surfaces, Appl. Surf. Sci. 440 (2018) 570–579. https://doi.org/10.1016/j.apsusc.2018.01.174.

[21] L.-Z. Hsieh, H.-H. Ko, P.-Y. Kuei, C.-Y. Lee, Growth Evolution of ZrO2 from Deposited Zr Metal during Thermal Oxidation, Jpn. J. Appl. Phys. 45 (2006) 7680–7681. https://doi.org/10.1143/JJAP.45.7680.

[22] S. Balakumar, R. Ajay Rakkesh, A.K. Prasad, S. Dash, A.K. Tyagi, Nanoplatelet structures of MoO 3 for H 2 gas sensors, Proc. Int. Conf. Nanosci. Eng. Technol. ICONSET 2011. (2011) 514–517. https://doi.org/10.1109/ICONSET.2011.6168019.

[23] G. Mestl, P. Ruiz, B. Delmon, H. Knozinger, H. Knözinger, Oxygen-exchange properties of MoO3: An in situ Raman spectroscopy study, J. Phys. Chem. 98 (1994) 11269–11275. https://doi.org/10.1021/j100095a007.

[24] A.S. Foster, A.L. Shluger, R.M. Nieminen, Mechanism of Interstitial Oxygen Diffusion in Hafnia, Phys. Rev. Lett. 89 (2002) 1–4. https://doi.org/10.1103/PhysRevLett.89.225901.

[25] C.R. Stilhano Vilas Boas, A.A. Zameshin, J.M. Sturm, F. Bijkerk, The influence of oxygen on the neutralization of slow helium ions scattered from transition metals and aluminum surfaces, Surf. Sci. 700 (2020) 121680. https://doi.org/10.1016/j.susc.2020.121680.

[26] H. Téllez, R.J. Chater, S. Fearn, E. Symianakis, H.H. Brongersma, J.A. Kilner, Determination of 16O and 18O sensitivity factors and charge-exchange processes in low-energy ion scattering, Appl. Phys. Lett. 101 (2012) 151602. https://doi.org/10.1063/1.4758699.

[27] M. De Ridder, R.G. Van Welzenis, H.H. Brongersma, U. Kreissig, Oxygen exchange and diffusion in the near surface of pure and modified yttria-stabilised zirconia, Solid State Ionics. 158 (2003) 67–77. https://doi.org/10.1016/S0167-2738(02)00759-2.

[28] J.B. Malherbe, S. Hofman, J.M. Sanz, Preferential sputtering of oxides: a comparison of model predictions with experimental data, Appl. Surf. Sci. 27 (1986) 355–365.

[29] C.R. Stilhano Vilas Boas, J.M. Sturm, F. Bijkerk, Oxidation of metal thin films by atomic oxygen : A low energy ion scattering study, J. Appl. Phys. 126 (2019) 155301. https://doi.org/10.1063/1.5115112.

[30] N. Cabrera, N.F. Mott, Theory of the oxidation of metals, Rep. Prog. Phys. 12 (1949) 163–184. https://doi.org/10034-4885/12/1/308.

[31] P. Gorai, A.G. Hollister, E.G. Seebauer, Electrostatic drift effects on near-surface defect distribution in TiO 2, Appl. Phys. Lett. 103 (2013). https://doi.org/10.1063/1.4824614.

[32] M. Kröger, S. Hamwi, J. Meyer, T. Riedl, W. Kowalsky, A. Kahn, Role of the deep-lying electronic states of MoO3 in the enhancement of hole-injection in organic thin films, Appl. Phys. Lett. 95 (2009) 1–4. https://doi.org/10.1063/1.3231928.

[33] J. J. B. Wachtman, A.D. Franklin, Mass Transport In Oxides, National Bureau of Standards, Washington, D.C., 1968.

[34] N.F. Mott, The theory of crystal rectifiers, 1 (1939) 153–165. https://doi.org/10.1142/9789812794086_0013.

[35] M. Lampimäki, V. Zelenay, A. Křepelová, Z. Liu, R. Chang, H. Bluhm, M. Ammann, Ozone-induced band bending on metal-oxide surfaces studied under environmental conditions, ChemPhysChem. 14 (2013) 2419–2425. https://doi.org/10.1002/cphc.201300418.

[36] R.A. De Souza, A universal empirical expression for the isotope surface exchange coefficients (k*) of acceptor-doped perovskite and fluorite oxides, Phys. Chem. Chem. Phys. 8 (2006) 890–897. https://doi.org/10.1039/b511702j.

[37] P. Gorai, E. Ertekin, E.G. Seebauer, Surface-assisted defect engineering of point defects in ZnO, Appl. Phys. Lett. 108 (2016). https://doi.org/10.1063/1.4953878.

[38] P. Fielitz, G. Borchardt, On the accurate measurement of oxygen self-diffusivities and surface exchange coefficients in oxides via SIMS depth profiling, Solid State Ionics. 144 (2001) 71–80. https://doi.org/10.1016/S0167-2738(01)00893-1.

[39] R.J. Friauf, Correlation effects for diffusion in ionic crystals, J. Appl. Phys. 33 (1962) 494–505. https://doi.org/10.1063/1.1777148.

[40] P. Phadke, C.R. Stilhano Vilas Boas, J.M. Sturm, R.W.E. van de Kruijs, F. Bijkerk, Near-threshold, steady state interaction of oxygen ions with transition metals: Sputtering and radiation enhanced diffusion, Appl. Surf. Sci. 518 (2020) 146143. https://doi.org/10.1016/j.apsusc.2020.146143.

[41] A.D. McNaught, A. Wilkinson, Compendium of chemical terminology, Blackwell Science Oxford, 1997.

[42] J. Yang, M. Youssef, B. Yildiz, Oxygen self-diffusion mechanisms in monoclinic Zr O2 revealed and quantified by density functional theory, random walk analysis, and kinetic Monte Carlo calculations, Phys. Rev. B. 97 (2018) 1–7. https://doi.org/10.1103/PhysRevB.97.024114.

[43] K. Inzani, T. Grande, F. Vullum-Bruer, S.M. Selbach, A van der Waals Density Functional Study of MoO3 and Its Oxygen Vacancies, J. Phys. Chem. C. 120 (2016) 8959–8968. https://doi.org/10.1021/acs.jpcc.6b00585.

[44] M.P. Mitoraj, A. Michalak, On the asymmetry in molybdenum-oxygen bonding in the MoO3structure: ETS-NOCV analysis, Struct. Chem. 23 (2012) 1369–1375. https://doi.org/10.1007/s11224-012-0056-5.

[45] R. Meyer, R. Waser, Observation of Vacancy Defect Migration in the Cation Sublattice of Complex Oxides by 18 O Tracer Experiments, Phys. Rev. Lett. 90 (2003) 1–4. https://doi.org/10.1103/PhysRevLett.90.105901.

[46] R.A. De Souza, M. Martin, Using18O/16O exchange to probe an equilibrium space-charge layer at the surface of a crystalline oxide: Method and application, Phys. Chem. Chem. Phys. 10 (2008) 2356–2367. https://doi.org/10.1039/b719618k.

[47] H. Ibach, Physics of surfaces and interfaces, 2006. https://doi.org/10.1007/3-540-34710-0.

[48] P. Gorai, A.G. Hollister, E.G. Seebauer, Measurement of Defect-Mediated Oxygen Self-Diffusion in Metal Oxides, ECS J. Solid State Sci. Technol. 1 (2012) Q21–Q24. https://doi.org/10.1149/2.011202jss.

[49] J. Fleig, Voltage-assisted 18O tracer incorporation into oxides for obtaining shallow diffusion profiles and for measuring ionic transference numbers: basic considerations, Phys. Chem. Chem. Phys. 11 (2009) 3010. https://doi.org/10.1039/b905911n.

[50] W.M. Haynes, CRC Handbook of Chemistry and Physics, 95th ed., CRC Press, 2014.

[51] J. Buckeridge, C.R.A. Catlow, M.R. Farrow, A.J. Logsdail, D.O. Scanlon, T.W. Keal, P. Sherwood, S.M. Woodley, A.A. Sokol, A. Walsh, Deep vs shallow nature of oxygen vacancies and consequent n -type carrier concentrations in transparent conducting oxides, Phys. Rev. Mater. 2 (2018) 56–59. https://doi.org/10.1103/PhysRevMaterials.2.054604.

[52] Ş. Baturay, A. Tombak, D. Batibay, Y.S. Ocak, n-Type conductivity of CuO thin films by metal doping, Appl. Surf. Sci. 477 (2019) 91–95. https://doi.org/10.1016/j.apsusc.2017.12.004.

[53] H. Peelaers, M.L. Chabinyc, C.G. Van De Walle, Controlling n-Type Doping in MoO3, Chem. Mater. 29 (2017) 2563–2567. https://doi.org/10.1021/acs.chemmater.6b04479.

[54] R.A. De Souza, Limits to the rate of oxygen transport in mixed-conducting oxides, J. Mater. Chem. A. 5 (2017) 20334–20350. https://doi.org/10.1039/c7ta04266c.

[55] J. Jamnik, J. Maier, S. Pejovnik, Interfaces in solid ionic conductors: Equilibrium and small signal picture, Solid State Ionics. 75 (1995) 51–58. https://doi.org/10.1016/0167-2738(94)00184-T.

[56] U. Brossmann, R. Würschum, U. Södervall, H.-E. Schaefer, Oxygen diffusion in ultrafine grained monoclinic ZrO2, J. Appl. Phys. 85 (1999).

[57] P. Gorai, E.G. Seebauer, Electric field-driven point defect pile-up near ZnO polar surfaces, Solid State Ionics. 301 (2017) 95–98. https://doi.org/10.1016/j.ssi.2017.01.015.

[58] P. Gorai, E.G. Seebauer, Kinetic model for electric-field induced point defect redistribution near semiconductor surfaces, Appl. Phys. Lett. 105 (2014). https://doi.org/10.1063/1.4890472.

[59] L.P.H. Jeurgens, W.G. Sloof, F.D. Tichelaar, E.J. Mittemeijer, Growth kinetics and mechanisms of aluminum-oxide films formed by thermal oxidation of aluminum, J. Appl. Phys. 92 (2002) 1649–1656. https://doi.org/10.1063/1.1491591.

Figure 1: XRD measurements of reactively deposited oxide samples. Main peaks corresponding to monoclinic ZrO_2 and orthorhombic MoO_3 are indicated with dashed lines. The curves intensity are shifted for clarity.

Figure 2: LEIS measurements of as deposited (purple) and 25 min $^{18}O_2$ exposed (red) (a) 3 nm ZrO_2 and (b) 3 nm MoO_3.

Figure 3: LEIS measurements of 20 nm MoO_3 as deposited (purple) and after exposure to atomic ^{18}O for 10 min (red).

Figure 4: Isotope profiles of samples exposed to ^{18}O after selected exposure time for (a) 3 nm ZrO_2, (b) 20 nm ZrO_2, (c) 3 nm MoO_3 and (d) 20 nm MoO_3. The red lines represent the calculated diffusion profiles at the saturation exposure time (100s for ZrO_2 and 450s for MoO_3) using Eq. (2) with parameters presented in **Error! Reference source not found.**.

Figure 5: Comparison between experimental (blue circles) and calculated evolution of surface ^{18}O concentration as a function of exposure time. (a) 3 nm ZrO_2 (b) 20 nm ZrO_2 (c) 3 nm MoO_3 (d) 20 nm MoO_3. Both continuous (red) and dotted (grey) lines are obtained with values presented in ***Error! Reference source not found.***. The red lines refer to calculations (discussed in sections 4.1 and 4.2) considering complete surface coverage/exchange, while grey dotted lines refer to calculations with limiting surface exchange values.

Figure 6: Schematic diagram of the effect of oxygen chemisorption, on surface charge distribution for a n-type oxides. (a) Flat band model: before oxygen exposure. (b) Band model representing the effect of oxygen chemisorption on band bending, and consequent interaction of isotopic oxygen (^{18}O - purple) with oxygen in the oxide lattice (^{16}O - blue) and vacancies (red squares).

Table 1: Values describing experimental data with results presented in red on Figures 4 and 5.

	Input parameters	Best fit parameters			Calculated parameters
	SCR (nm)	N_d (m^{-3})	Φ_0 (eV)	k_e^* (m s^{-1})	D_e^* (m^2 s^{-1})
3 nm ZrO_2	1.2	4.1×10^{-26}	- 0.28	4.5×10^{-12}	9.2×10^{-22}
20 nm ZrO_2	1.0	4.0×10^{-26}	- 0.28	3.6×10^{-12}	5.5×10^{-22}
3 nm MoO_3	2.3	2.1×10^{-26}	- 0.28	2.3×10^{-12}	9.2×10^{-22}
20 nm MoO_3	2.5	1.8×10^{-26}	- 0.29	2.9×10^{-12}	1.2×10^{-21}